Microstructure, Texture, and Tensile Properties of Ultrafine/Nano-Grained Magnesium Alloy Processed by Accumulative Back Extrusion

S.M. FATEMI, A. ZAREI-HANZAKI, and J.M. CABRERA

An AZ31 wrought magnesium alloy was processed by employing multipass accumulative back extrusion process. The obtained microstructure, texture, and room temperature tensile properties were characterized and discussed. Ultrafine-grained microstructure including nano-grains were developed, where the obtained mean grain size was decreased from 8 to 0.5 μm by applying consecutive passes. The frequency of both low angle and high angle boundaries increased after processing. Strength of the experimental alloy was decreased after processing, which was attributed to the obtained texture involving the major component lying inclined to the deformation axis. Both the uniform and post-uniform elongations of the processed materials were increased after processing, where a total elongation of 68 pct was obtained after six-pass deformation. The contribution of different twinning and slip mechanisms was described by calculating corresponding Schmid factors. The operation of prismatic slip was considered as the major deformation contributor. The significant increase in post-uniform deformation of the processed material was discussed relying on the occurrence of grain boundary sliding associated with the operation of prismatic slip.

I. INTRODUCTION

MAGNESIUM and its alloys exhibit poor formability and negligible hardenability at room temperature, which impede their potential application for automobile, electronic, and aerospace industries.[1] Thus, to employ their merits over many structural materials including superior specific stiffness and strength, the low-temperature hardenability and ductility of magnesium alloys should be improved. Two promising ways in this direction are the grain refinement[2,3] and manipulation of crystallographic texture.[4,5] In large-grain magnesium, basal slip facilitates microscopic yielding at very low stress. In order to accommodate further deformation, other slip systems should be activated. Koike et al.[6] showed that, in fine-grained magnesium, the dislocation cross-slip to non-basal planes occurred at very low stress level due to grain boundary compatibility stress. The substantial dislocation activity on non-basal planes brought about a respectful room temperature tensile ductility. Moreover, the low symmetry HCP crystal structure makes magnesium alloys very sensitive to crystallographic texture in such a way that their mechanical properties vary considerably with changes in sample orientation.[7,8] Activation of different slip and twinning systems is primarily influenced by the initial orientation. For ductilizing magnesium, the initial texture should be tailored ensuring that the Schmid factor (SF) for the basal slip is maximized.[9]

Severe plastic deformation (SPD) processes are considered to improve room temperature mechanical properties in magnesium alloys, e.g., References 5 and 10. During SPD, the initial grain size of the material is significantly reduced by thermally aided plastic deformation through different recrystallization mechanisms.[10,11]

As deformation and grain refinement may also cause variations in crystallographic texture, the post-SPD mechanical properties result from combined effects of grain refinement and texture changes. Furthermore, it has been demonstrated that the degree of grain refinement by SPD, itself, is strongly coupled to the development of texture and substructural evolutions.[12,13] It has been proposed that grain refinement is primarily the result of the interaction of shear plane with texture and the crystal structure, followed by an influence coming from the accumulation of shear strain during severe deformation.[12] It has been known that moderate-to-strong level of complex textures can be induced during SPD of magnesium alloys.[14,15]

SPD methods have been examined in several studies to explore the possibility of inducing improved low-temperature strength and ductility in magnesium alloys, e.g., Reference 16. Reported results on the mechanical properties of SPDed magnesium alloys illustrated that a miscellaneous combination of strength and ductility alterations may be obtained, depending on synergistic or

S.M. FATEMI is with the School of Mechanical Engineering, Shahid Rajaee Teacher Training University, 136-16785, Tehran, Iran. Contact e-mail: mfatemi@ut.ac.ir A. ZAREI-HANZAKI is with the Department of Metallurgical & Materials Engineering, University of Tehran, 515-14395, Tehran, Iran. J.M. CABRERA is with the Departamento de Ciencia de Materiales e Ingeniería Metalúrgica, ETSEIB, Polytecnic University of Catalonia, Av. Diagonal, 647-08028, Barcelona, Spain.
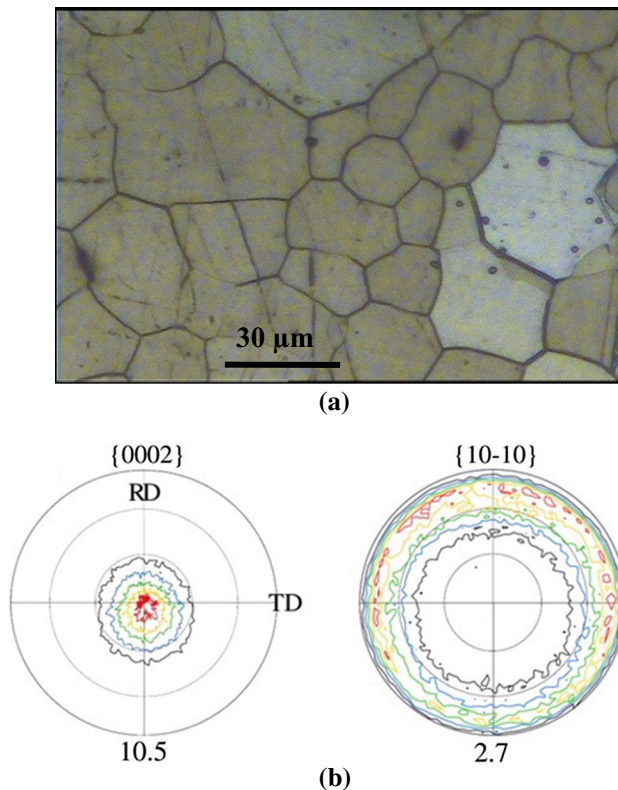
Fig. 1—(a) Initial microstructure, (b) measured pole figures of the experimental as-rolled AZ31 alloy.

occurrence of grain boundary sliding (GBS) plays a key role in low strain rate deformation of fine-grained pure magnesium. However, Wang and Ma[25] suggested that the design and processing of a bimodal or even multi-modal grain structure is a profitable approach for developing new materials. They made the point that a uniform and extremely fine nanocrystalline structure is neither necessary nor beneficial for properties and applications, if a high ductility, in addition to the high yield strength, is desired. Although the reported works accentuated on the effect of texture changes and grain refinement on the final properties, rare research could be found in the literature dealing with the detailed discussion on the role of different deformation mechanisms as well as microstructure refinement on the mechanical properties of magnesium SPD products.

A new continuous SPD process, the so-called accumulative back extrusion process (ABE), which is an appropriate technique for the production of ultra-fine/nano-grained bulk material has been introduced in recent years.[27–29] Previous works mainly dealt with the developed strain patterns,[30] microstructural evolutions,[29] homogeneity,[31] and texture evolution[32] during ABE processing. In this work, the tensile properties of an AZ31 magnesium alloys processed by accumulative back extrusion (ABE) were examined. Moreover, the effect of microstructure and texture evolution on the final mechanical properties of the ultra/fine-grained magnesium was described relying on the contribution of different deformation mechanisms.

II. EXPERIMENTAL PROCEDURE

A commercial AZ31 alloy (Mg-2.9Al-0.9Zn-0.7Mn, wt pct), received in the form of rolled plate, was used as experimental alloy. Cylindrical samples for ABE processing were machined with the dimensions of H8 × Φ18 mm^2. Briefly, the first step of ABE consists of the back extrusion of the workpiece into the gap between the inner punch and the die. In the second step, the back extruded material is forged back to the initial cross section by the outer punch completing one ABE cycle. The previous work showed that an average equivalent strain of 2 is induced during each step.[30] ABE process was conducted at a ram speed of 5 mm/min and temperature of 553 K (280 °C). According to the relatively low stroke speed, the temperature increasing during extrusion was ignored. The MoS2 spray was used to reduce the friction between the work piece and the tool surfaces. The initial material showed a mean grain size of 25 μm (Figure 1(a)). Crystallographic texture measurements were conducted using X-ray diffraction in the reflection geometry with a four circle goniometer and Cu Ka radiation. Experimental (1 0 −1 0), (0 0 0 2), and (1 0 −1 1), pole figures were collected on a 5 × 5 deg grid for sample tilts, α = 0–85 deg, and azimuthal rotations, φ = 0–355 deg. Background and defocusing corrections were made using experimentally determined data from random powder samples. The texture of initial material is illustrated in Figure 1(b),
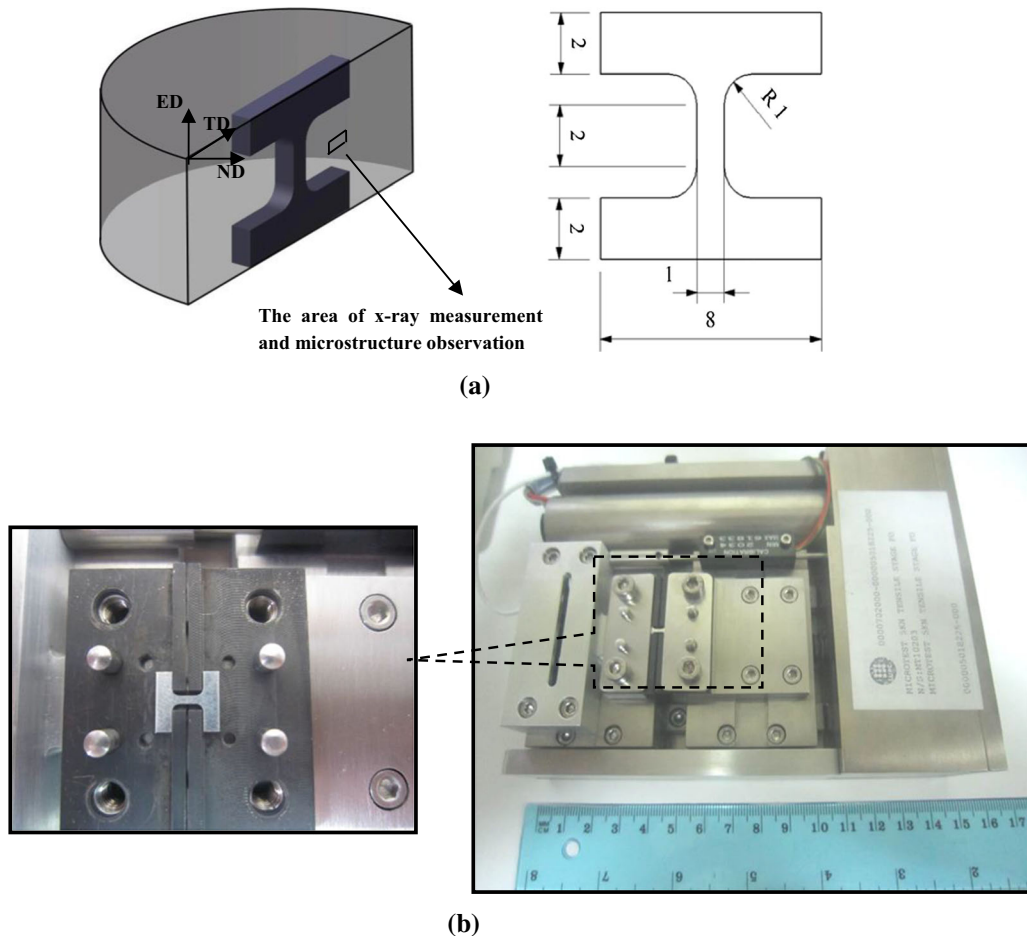
antagonistic effects of grain refining and texture change.[17–20] Furthermore, it was recognized that the Hall–Petch parameters are texture dependent so that easy activation of basal slip introduces lower values, while inhibition of basal slip leads to higher values.[20] Xing et al.[21] and Zuberova et al.[22] reported that SPD of AZ31 alloy gave rise to an increased strength accompanied by a minor ductility. The latter observations describe a case where the strengthening due to grain refinement is amplified by texture hardening, while the latter counteract the ductulizing effect of former. However, results of opposite trend were obtained by Kim et al.[23] where the yield stress of a wrought AZ61 alloy processed by eight equal channel angular pressing (ECAP) passes dropped appreciably as compared to the initial material, while the tensile ductility was significantly increased. Dissimilarly, the results reported by Miura et al.[24] on multi-axial forging of AZ61 alloy implied that although the tensile strength increased with a decrease in grain size and texture changes, the ductility was not spoiled.

It is generally accepted that grain refinement leads to a decrease in strain hardening as yield strength is increased;[25] however, Ghosh and Yang[26] believed that the combined effect of increased strain rate sensitivity and strain hardening may offset the loss in ductility in AZ31 magnesium alloy. In addition, microstructure features, such as grain boundary nature and dislocation structures, could have important effects on mechanical properties. Figueiredo et al.[19] showed that the

Fig. 2—(*a*) Schematic illustration of geometry and orientation of tension specimen used in mechanical testing, (*b*) tension machine for testing miniaturized samples.

where a strong fiber texture with most of the basal planes aligned parallel to the rolling direction (RD)–transverse direction (TD) plane. For all the ABE samples, the center of the rectangular cross section of ABEed sample was considered for representative metallographic observations. The microstructures of the deformed material were examined through optical microscopy and transmission electron microscopy (TEM). The TEM investigation was performed using a Philips CM 20 microscope working at 200 kV. Toward this purpose, a slice of the ABEed workpieces was first cut parallel to the extrusion direction. The slice was then thinned by grinding to a sheet with 100 μm thickness. The TEM samples were then mechanically polished using a twin-jet polishing unit. The perforation was done by a solution of 1 pct perchloric acid, 99 pct ethanol at a polishing temperature of 275 K. Electron back scattered diffraction (EBSD) was performed using scanning electron microscope (FEGSEM, Zeiss Ultra Plus) equipped with EBSD camera. The microstructural maps were derived from EBSD, which shows grains and sub-grains based on misorientation angle on adjacent points. To analysis microstructure, three scans were made over the cross section.

Because of the small size of the ABEed workpiece, miniaturized specimen was machined from the as-received and ABE-processed materials for tension testing with a gage section of $0.7 \times 1 \times 2$ mm, the longitudinal direction of which was selected to be parallel to the ABExtrusion (as shown in Figure 2(a)). For the as-received material, the tension samples were cut along the rolling direction. Tensile tests were performed on the samples using a Deden tension machine (Figure 2(b)) with a constant crosshead velocity of 0.02 mm/min providing an initial strain rate of about 17×10^{-5} s^{-1}. To verify the reproducibility of the results, three tension specimens were cut from the ABEed samples and tested.

III. RESULTS AND DISCUSSION

The microstructural observations demonstrated that an outstanding grain refinement took place through ABE processing, where a relatively homogeneous grain refinement was achieved after sixth pass. TEM observation showed that recrystallized areas include grains of 80 nm to 1 μm. Figures 3(a), (b), and (c) typically show the microstructure of the ABE-processed AZ31 alloy up
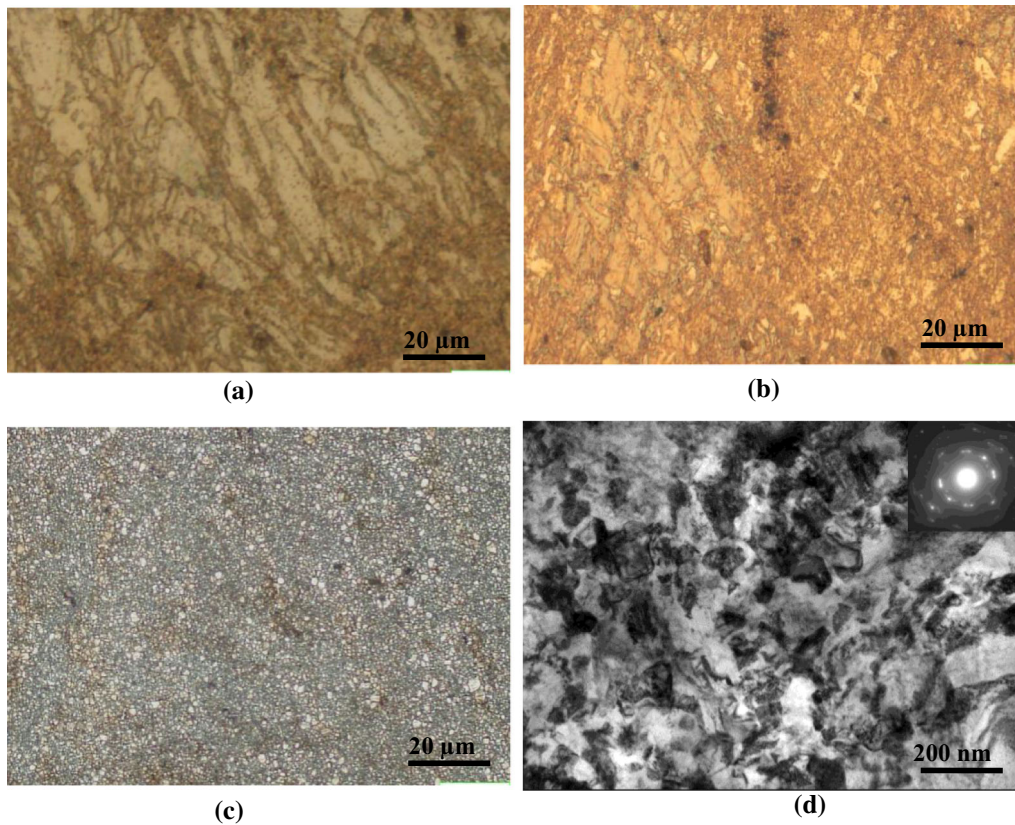
Fig. 3—Microstructure of the experimental alloy deformed up to (*a*) one, (*b*) two, (*c*) six passes at 553 K (280 °C), (*d*) ultrafine/nano-grains formed during ABE processing.

to one, two, and six passes, respectively. The ultrafine/nano-grains developed during deformation are depicted in Figure 3(d). As the experimental alloy was processed by successive passes, the coarse grain was substituted by fine recrystallized grains and more homogenous microstructure was obtained. The average grain sizes were measured to be about 8, 2, and 0.5 μm after processing of one, two, and six ABE passes, respectively. Figure 4 displays typical grain size distribution of the processed materials. As discussed in Reference 11, discontinuous dynamic recrystallization was found as the dominant grain refinement mechanism in AZ31 experimental alloy during the early ABE pass; thereafter the dynamically recrystallized grains, in turn, were repetitively refined through continuous dynamic recrystallization upon applying successive passes.

To understand the evolution of substructure and development of fine grains during successive ABE passes, EBSD maps of the material deformed up to different ABE passes were obtained from ED-TD plane. The results are presented in Figure 5, where formations of new grains as well as fragmentation of prior grains by subboundaries are evident. Figure 6 shows the distributions of the misorientation angles in terms of cumulative frequency (frequency of and below a given misorientation angle) of low angle boundaries (LABs) and high angle boundaries (HABs) in the samples ABEed at 553 K (280 °C). It indicates that the frequency of LABs with misorientation angles below 15 deg increased after single

ABE, which confirms the operation of extensive dynamic recovery. However, the frequency of LABs decreases but that of HABs increases with applying successive passes. The decrease in LABs (misorientation below 15 deg) may indicate the transformation of LABs to HABs by incorporating the dislocations that generate during deformation. The latter requires new grain boundary area to be continuously created during deformation.[33] This is consistent with the increase in frequency of HABs. Previous results showed that the microstructure is repetitively refined though subdivision of the DRXed grains into finer ones.[11]

The basal, prismatic, and pyramidal pole figures of the sample deformed by different ABE passes were measured. The results were presented elsewhere;[32] however, for the sake of convenience, the pole figures from the materials after the first and fourth passes are shown in Figure 7. As realized, the original texture (Figure 1(b)) was completely replaced and a new texture developed during the first pass. This is connected to the high shear strain magnitude imposed during ABE deformation.[30] The obtained ABE texture corresponds to the basal poles lying ~40 deg away from the TD in the ED–TD plane and 66 deg from the normal direction (ND) in the TD–ND plane, while the maximum of prismatic planes was appeared at inclination angle of 40–50 deg in the TD–ED plane. These texture components mostly place the magnesium crystal inclined to the ABE axis. The post-ABE texture may be discussed
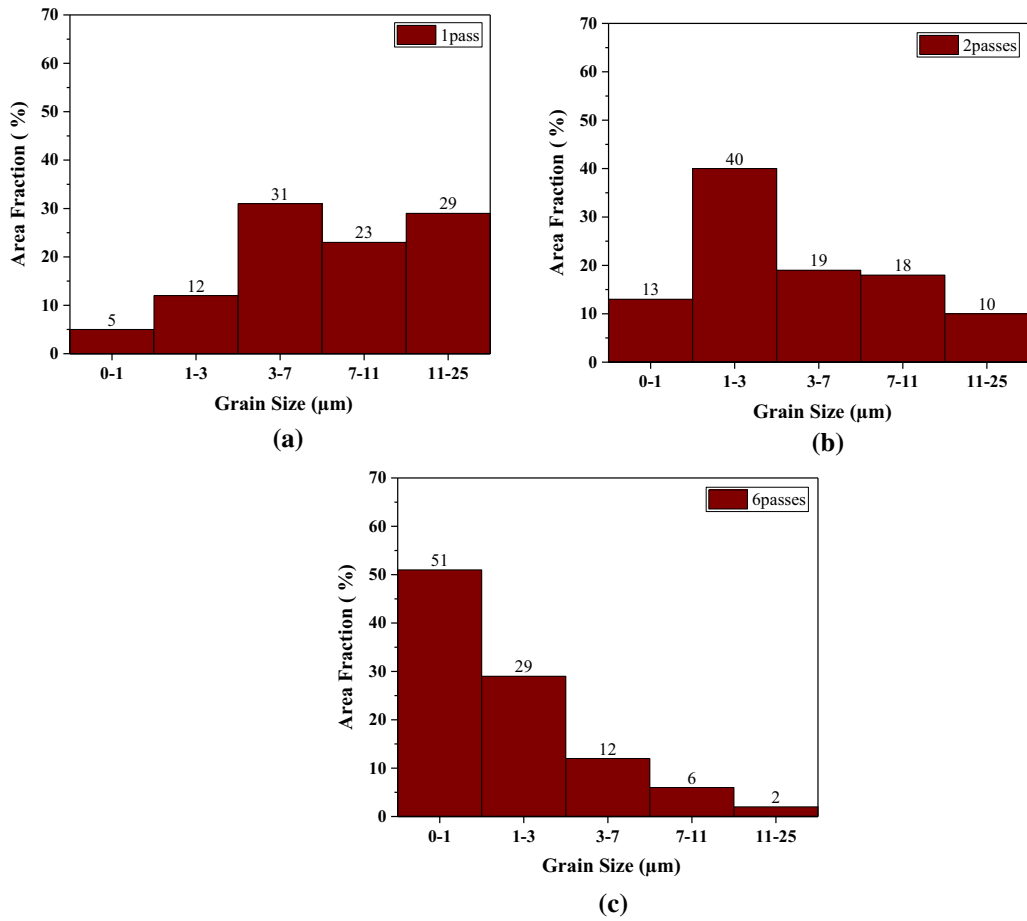
Fig. 4—Typical grain size distribution of the experimental alloy processed by (*a*) one pass, (*b*) two passes, and (*c*) six passes at 553 K (280 °C).
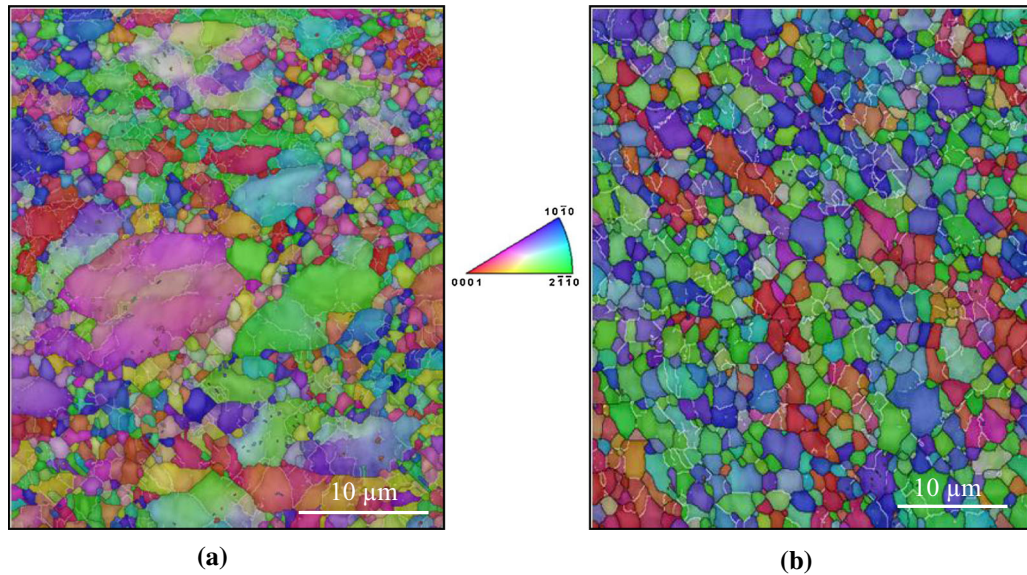

Fig. 5—Inverse pole figures of the material deformed up to (*a*) one pass, (*b*) four passes. White and black lines denoted boundaries with misorientation below and above 15 deg, respectively.
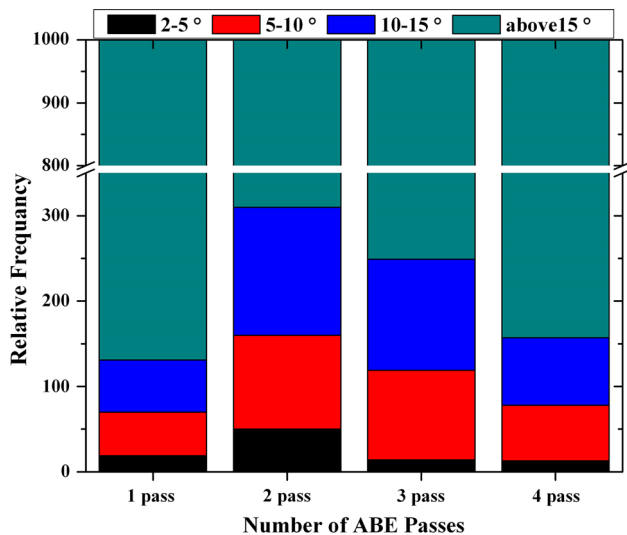
Fig. 6—Cumulative frequency of boundaries with different misorientation angle in AZ31 alloy deformed to various numbers of ABE passes.

relying on the presence of favorable initial basal texture, where the c-axis is mostly oriented by 40–50 deg from the shear direction during ABE.[32] With the application of subsequent passes, there is a tendency of the basal plane lying parallel to TD, while the orientation of prismatic planes shows a random distribution around ND. Accordingly, after four passes, it is evident that the most noticeable texture includes fiber basal texture oriented almost parallel to the transverse direction, and $\langle 1\,0\,{-}1\,0 \rangle$ perpendicular to the ED.

Figure 8(a) shows tensile stress *vs* strain for the coarse-grain as-received and UFG as-processed alloys at room temperature. However, one can readily notice that the mechanical properties were significantly altered after ABE deformation. The data of yield stress (YS), ultimate tensile strength (UTS), and fracture strain are summarized in Figure 8(b). The yield stress slightly drops after the first pass, and then increases as subsequent passes are applied. The UTS also decreased after the first pass, while it continues to ascend with increasing number of passes, where a UTS of 250 MPa was reached after six ABE passes. The elongation of processed material gradually increased where an exceptional ductility of about 68 pct was measured after multiple ABE passes. The correlation between grain size and yield stress based on Hall–Petch relation was established in Figure 9. It is obvious that the data belonging to the as-received alloy are out of line with the ones obtained from processed materials. The enhanced yield strength of the as-received alloy comparing the plotted Hall–Petch correlation is related to the different deformation modes dominating at the beginning of plasticity. This will be discussed later in this paper.

Considering the miniaturized tensile samples employed in this study, one may expect a greater post-uniform elongation comparing to standard samples. Gage length tends to have significant effects on the post-uniform elongation and the total ductility. The

shorter the gage length the greater the total elongation is expected.[26,34] Moreover, it has been found in the case of ultrafine-grained Cu that thicker specimens tend to be more ductile, too. The thickness effect is mainly caused by the necking geometry and/or fracture modes.[34] Thus, to compare results with the literature, the effect of specimen geometry should be considered. A method for determination of stable strain before maximum load for the as-processed alloy is using Considère construction:

$$\frac{d\sigma}{d\varepsilon} = \sigma, \quad [1]$$

where σ and ε refer to true stress and true strain. The variations of work hardening rates were included as dashed lines in Figure 8(a). The portions beyond the intersection point on the curves represent post-uniform deformation. It is evident that both uniform and non-uniform strains are improved in the fine-grained processed materials.

A power law constitutive relation ($\sigma = K\varepsilon^n$) is shown to fit the flow curves with reasonably accuracy for true-strains up to about 0.15 (Figure 10). The deviation from the linear relationship may be related to the changes in the share of different slip systems as the strain accommodation progressed and thus to the slight change in n value. The results implied that the hardening exponent (n) was slightly decreased after ABE processing, which is connected to the grain refinement effect. However, opposed to the grain refining effect, the evolution of texture caused a decrease in the yield stress as well as a slight increase in uniform elongations, as will be further discussed in the following paragraphs. A large post-uniform elongation is promoted by preventing localization of the deformation as a sharp neck. This may be introduced due to the increased rate of thermally activated processes such as dislocation climb and GBS.[35] The occurrence of GBS at ambient temperature was associated to a large strain rate sensitivity at the vicinity of the grain boundary.[36] Since the volume of grain boundaries increases with grain refinement, ultrafine and nano-grained magnesium may exhibit an extended non-uniform deformation. It is worth noting that total elongation was relatively deteriorated after the second pass (see Figure 8). This observation may be attributed to the increased frequency of LABs after the second pass. It was previously reported that the mechanism of strain propagation through boundaries with misorientations of <35 deg may limit strain accommodation by this mechanism.[37]

One way to quantify the texture data is to use the crystallite orientation distribution function (ODF), which essentially describes the frequency of the occurrence of particular orientations in a three-dimensional (Euler) orientation space. To identify the degree to which twinning and/or slip systems contribute during tensile deformation of ABEed materials, the ODFs were obtained from x-ray diffraction texture data on the basis of spherical harmonics with positivity correction according to Dahms and Bunge.[38] ODFs are typically depicted for one and two-pass processed materials in Figure 11. Accordingly, the crystallographic plane and
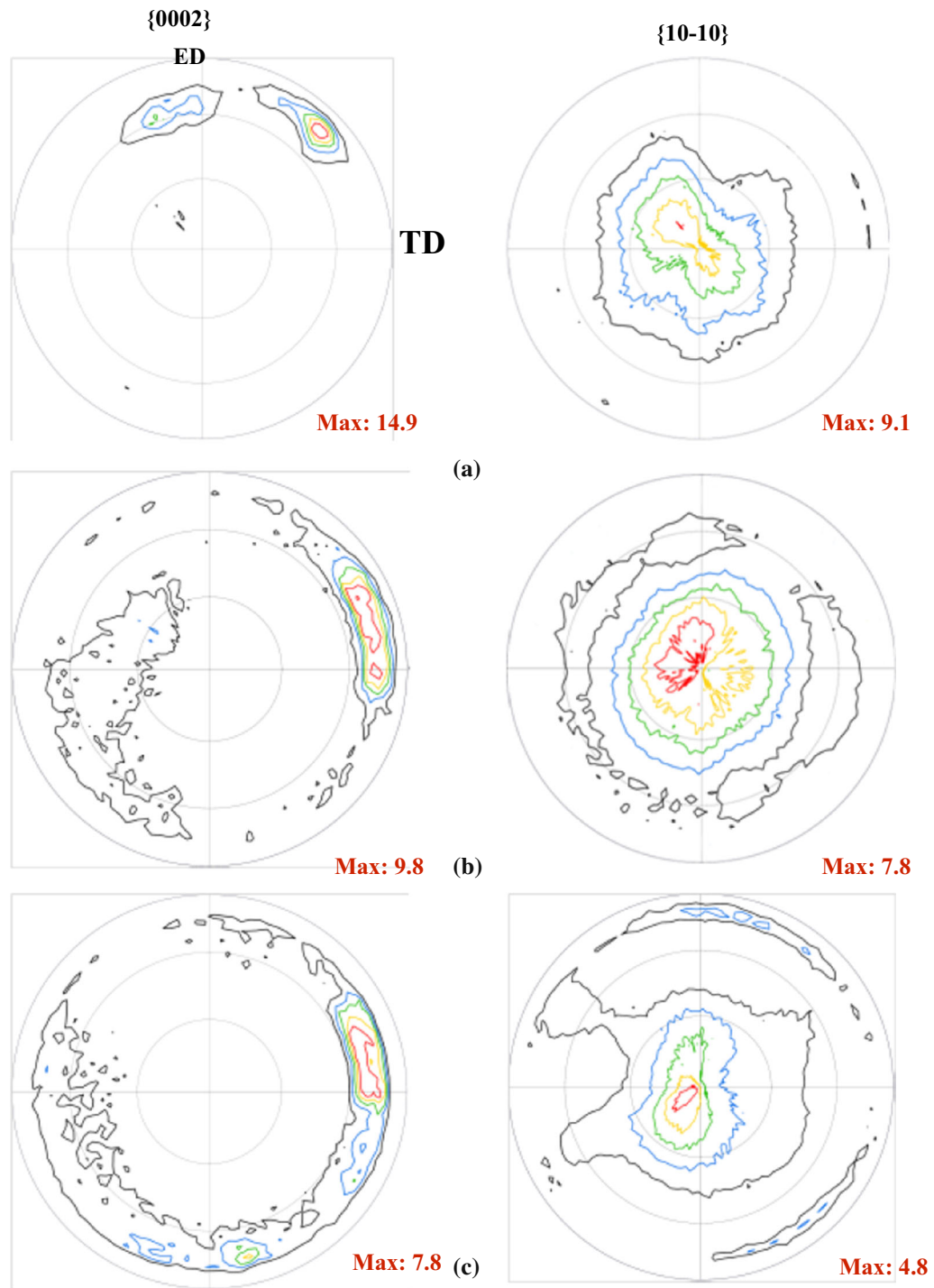
Fig. 7—(0 0 0 2) and (1 0 –1 0) pole figures of the texture of the experimental alloy ABEed up to (*a*) one pass, (*b*) four passes, (*c*) six passes. The maximum intensities, denoted as red lines, are presented below the figures as multiples of random density (mrd) (Color figure online).

direction which lie, in most of grains, parallel to the extrusion direction of ABEed samples (and thus parallel to tension axis) could be defined. The corresponding Euler angles, planes, and directions were given in Table I. The defined directions correspond to the deformation axis of the tension samples. The HCP crystal lattice of magnesium features the six equivalent twinning planes, the Schmid factors of which can be calculated numerically for any possible orientation in the textured polycrystalline alloy. For the twinning systems, the variant with maximum Schmid factor and for the slip systems the average values of Schmid factors
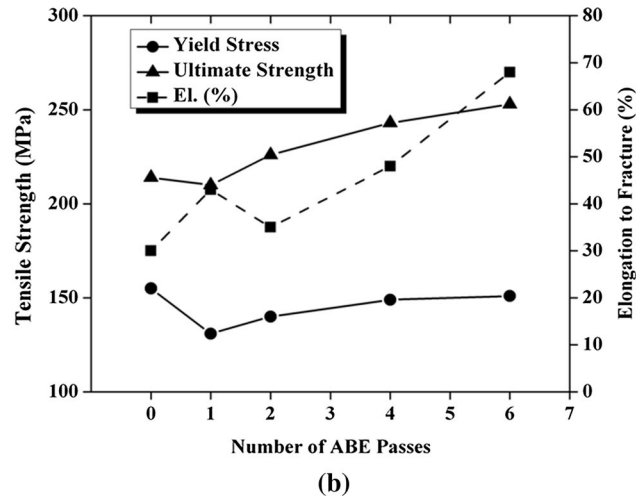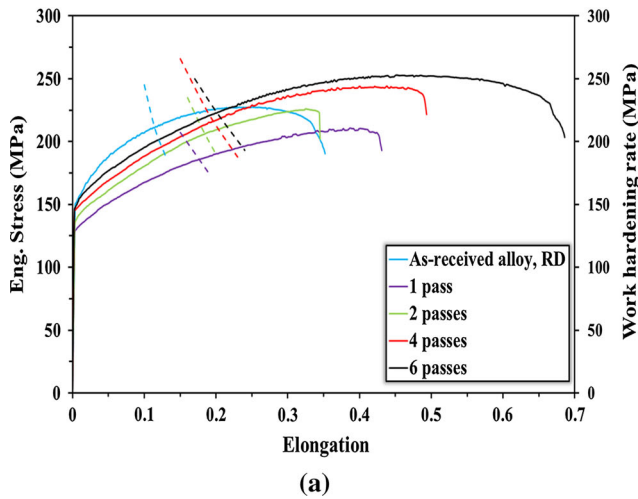
Fig. 8—(a) Tensile true stress vs true strain at room temperature for as-received and processed experimental alloy, (b) Variation of the yield stress, UTS and fracture strain with the number of ABE passes. The dashed lines are corresponding hardening rates.
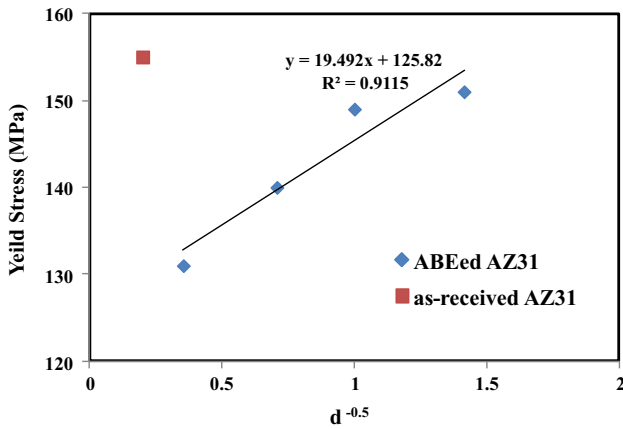

Fig. 9—The Hall–Petch correlation of yield stress and grain size for the as-received and processed alloys.
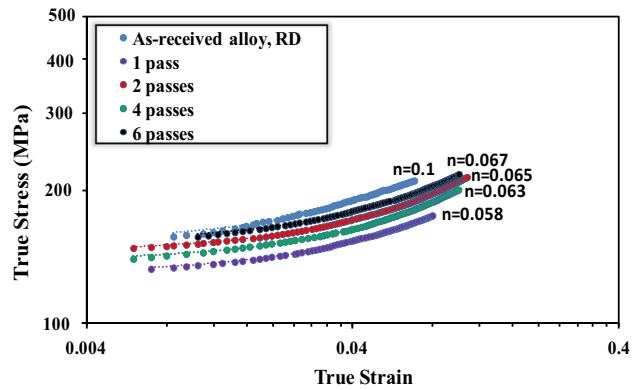

Fig. 10—Tensile data on a log–log plot exhibiting power law hardening for as-received and multipass processed AZ31 alloy.

were considered as effective Schmid factors. For the samples with two intensity peaks, the values proposed by the two were averaged out.

In the present paper, the system with the highest Schmid factor is supposed to become activated. For the as-received material, most grains have basal poles aligned almost perpendicular to the RD, maintaining a $\langle 1 \,{-}2\, 1\, 0\rangle$ pole peak parallel to the tension direction. As $\{1\, 0\, {-}1\, 2\}$-tensile twinning creates extension along the c-direction it cannot operate for tensile loads in the basal plane, though it possesses a proper absolute values of Schmid factor for activation. The latter refers to a case of negative Schmid factor for twinning system. So, the texture of initial rolled material does not favor the tensile twinning during RD tension. Also, as the Schmid factor is not appropriate to activate basal slip, the constraint of the limited number of independent slip systems causes a high yield stress. The flow stress increases to reach critical shear stress for prismatic slips, which are favored with Schimd factor of 0.37. Moreover, c + a slip having Schimd factor of 0.17 may also contribute at higher strain to contract the material along

c-axis.[39] The strain hardening behavior observed along the RD is consistent with the suppression of twins, where monotonic exhausted hardening rate was recorded. The latter hardening behavior led to a "convex" shape of flow curve with respect to the upper end of the stress axis (see Figure 8).

As the material processed through single-pass ABE, the Schmid factor calculated for the activation of twinning is lowered but yet considerable, according to Table I. However, it should be noted that due to the grain refinement introduced during ABE, the critical stress required for twinning significantly increases. Thus, twinning may hardly be involved during tensile tests of ABEed materials. Previous works have denoted that the occurrence of twinning is stopped in AZ31 alloy at a grain size of 3 μm[26,40] and 3.4 μm.[41]

The main texture components of the processed alloy have the c-axis of most of the grains distributed inclined to the ABExtrusion direction, though it tends to rotate toward transverse direction with increasing number of passes (Figure 7). This orientation is commonly described as a soft orientation that is favorable for easy
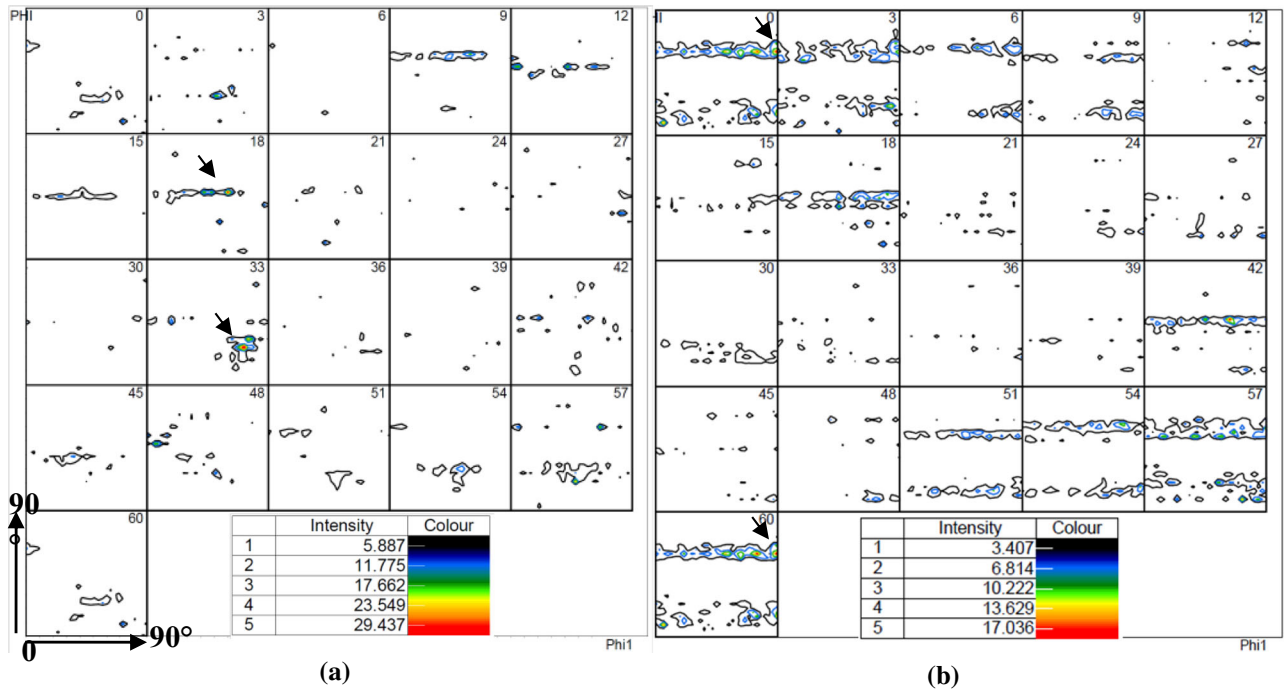
Fig. 11—ODF sections of different φ_2 values measured from the processed AZ31 alloy ABEed up to (*a*) one pass, (*b*) two passes. Strongest intensities were arrowed.

slip modes. According to Table I, the activation of basal slip system is favored after ABE processing. Thus, easy glide on basal planes may be considered as the primary deformation mechanism. The critical resolved stress for activation of basal slip is much less than prismatic one.[42] This fact may help to explain the drop in the yield stress, governing the occurrence of slip during tensile loading of ABEed materials. These evidences implied that the texture softening resulted from ABE texture overcomes the hardening effect generated by grain refinement. The fraction of dynamic recrystallization increased with applying consecutive passes, and the mean grain size of the ABEed alloy markedly lowered. This may harden the material by impeding basal slips and grain boundary strengthening effect. Moreover, the latter can be amplified by weakening of the basal texture intensity, which limits, in turn, the share of easy glide on basal plane during deformation. As the tensile deformation of ABEed samples progresses and hardening occurs on basal planes, prismatic slip can be contributed in deformation. According to the initial texture in tension samples, a $\langle 1\ -1\ 2\ 0 \rangle$ prismatic slip may accommodate the plastic strain through contraction in the thickness direction. Moreover, $\langle 1\ -1\ 0\ 0 \rangle$ double slip (*i.e.*, concurrent activation of two prismatic slip systems; *e.g.*, $(0\ 1\ -1\ 0)\ [2\ -1\ -1\ 0]$ and $(1\ -1\ 0\ 0)\ [1\ 1\ -2\ 0]$) may incorporate in the elongation of the sample. Detailed discussion of double prismatic slip in textured magnesium can be found in the work published by Saxl *et al.*[43] Thus, prismatic slip as the major deformation mechanism renders the shape change favored during tension test. A significant role of double prismatic slip in enhancing the ductility of magnesium alloys was previously reported by Kainer *et al.*[44] and Al-Samman *et al.*[8] Accordingly, the operation of prismatic slip results in the orientation of individual grains remaining virtually unchanged during deformation.[8] Moreover, GBS also occurs at room temperature up to 8 pct of total strain, enhanced by plastic anisotropy as well as by the increasing number of grain-boundary dislocations.[39] GBS at room temperature is related to slip-induced inhomogeneous plastic deformation of the ultrafine/nano-grained processed material. The positive role of GBS in enhancing ductility should be associated with the activity of non-basal slips.[6,39] In present work, the desired orientation condition for operation of prismatic slip systems and thereby concentrated stresses at the grain boundaries caused by dislocation slip invoke the occurrence of GBS. This mechanism is considered to give rise to considerable ductility improvement in ultrafine/nano-grained ABEed magnesium. As the number of passes increased, further reducing of the mean grain size as well as improving the Schmid factor for operation of prismatic slip resulted in a promoted boundary sling associating with a significant ductility of 68 pct. Somekawa and Mukai[45] showed a superplastic elongation of 230 pct at room temperature and strain rate 10^{-5} s^{-1} in pure Mg having a mean grain size of 1.2 μm. More recently, excellent ductilities were recorded in pure magnesium with even finer grain structures including an elongation of 360 pct in a sample with a grain size of 320 nm tested at room temperature at a low strain rate of 10^{-5} s^{-1}.[19] The latter improved ductilities were also attributed to an enhanced contribution from grain boundary sliding to the overall deformation mechanism.

Table I. Absolute Values of Schmid Factors Calculated for Twinning and Slip Systems in the Processed AZ31 Alloy Assuming the Axis of ABEed Sample as Deformation Axis

Pass Number	g{φ₁,φ,φ₂}	Deformation	Twinning	Max.	Ave.	Basal Slip	Average	Prismatic Slip	Average	Pyramidal Slip	Average
0	{81,0,12} {81,0,57}	≅ (0001)⟨1̄210⟩	0.24, 0.42,0.42 / 0.00,0.24, 0.00	0.42	0.42	0.00, 0.00, 0.00	0.00	0.00, 0.45, 0.27	0.37	0.22, 0.07, 0.22	0.17
1	{72,63,33}	≅ (011̄1)⟨12̄1̄1⟩	0.26, 0.28, 0.24 / 0.19, 0.28, 0.21	0.21	0.21	0.07, 0.23, 0.00	0.15	0.02, 0.07, 0.00	0.03 0.06	0.03, 0.13, 0.01 0.06	0.06
	{60,45,18}	≅ (011̄1)⟨1̄101⟩	0.10, 0.21, 0.21 / 0.14, 0.14, 0.03	0.21		0.30, 0.34, 0.07	0.22	0.00, 0.23, 0.07	0.10	0.04, 0.16, 0.06 0.09	0.09
2	{90,30,0}	≅ (1̄21̄1)⟨1̄211⟩	0.12, 0.19, 0.00 / 0.07, 0.17, 0.00	0.19	0.28	0.15, 0.43, 0.22	0.27	0.10, 0.32, 0.00	0.14	0.00, 0.10,0.16 0.09	0.09
	{90,30,60}	≅ (112̄1)⟨1̄121⟩	0.18, 0.19, 0.07 / 0.34, 0.04, 0.37	0.37		0.27, 0.33, 0.42	0.34	0.01, 0.23, 0.17	0.14	0.04, 0.16, 0.04 0.08	0.08
4	{69,45,18} {39,45,18}	≅ (011̄1)⟨1̄101⟩	0.22, 0.11, 0.39 / 0.1., 0.23, 0.19	0.39	0.39	0.39	0.24, 0.35, 0.08	0.30, 0.04, 0.14	0.18	0.07, 0.15, 0.00	0.07
6	{0,,60,30}	≅ (011̄1)⟨21̄1̄0⟩	0.27, 0.00, 0.27 / 0.00, 0.41, 0.41	0.41	0.45	0.00, 0.00, 0.00	0.00	0.04, 0.28, 0.22	0.21	0.07, 0.07, 0.26 0.13	0.11
	{90,60,18}	≅ (011̄1)⟨01̄11⟩	0.18, 0.27, 0.28 / 0.23, 0.37, 0.49	0.49		0.03, 0.21, 0.12	0.12	0.00, 0.04, 0.00	0.02	0.06, 0.12, 0.00 0.09	0.09

For the twinning systems the variant with maximum Schmid factor and for the slip systems the average values of Schmid factors were considered as effective Schmid factors. For the samples with two intensity peaks, the values proposed by the two were averaged out.

IV. SUMMARY

Ultrafine/nano-grained microstructure was produced in AZ31 wrought magnesium alloy through multipass ABE processing. A texture involving major texture component inclined to the deformation axis was developed. The promotion of easy basal slip due to the texture changes counteracts the strengthening effect of grain refinement, where the yield stress of the experimental material reduced after processing. The contribution of different twinning and slip systems during room temperature tension of ABEed alloys was discussed relying on the Schmid factor calculated by considering the obtained texture. Both uniform and post-uniform elongations of the material were improved after processing. The occurrence of GBS associated with the operation of prismatic slip results in a significant post-uniform elongation.

REFERENCES

1. B. Mordike and T. Ebert: *Mater. Sci. Eng. A*, 2001, vol. 302, pp. 37–45.
2. T. Al-Samman and G. Gottstein: *Mater. Sci. Eng. A*, 2008, vol. 488, pp. 406–14.
3. H. Yan, R. Chen, and E. Han: *Mater. Sci. Eng. A*, 2010, vol. 527, pp. 3317–22.
4. S. Agnew, J. Horton, T. Lillo, and D. Brown: *Scripta Mater*, 2004, vol. 50, pp. 377–81.
5. J. Del Valle, F. Carreno, and O. Ruano: *Acta Mater.*, 2006, vol. 54, pp. 4247–59.
6. J. Koike, T. Kobayashi, T. Mukai, H. Watanabe, M. Suzuki, K. Maruyama, and K. Higashi: *Acta Mater.*, 2003, vol. 51, pp. 2055–65.
7. S. Agnew, P. Mehrotra, T. Lillo, G. Stoica, and P. Liaw: *Mater. Sci. Eng. A*, 2005, vol. 408, pp. 72–78.
8. T. Al-Samman, X. Li, and S.G. Chowdhury: *Mater. Sci. Eng. A*, 2010, vol. 527, pp. 3450–63.
9. S. Biswas, S. Singh Dhinwal, and S. Suwas: *Acta Mater.*, 2010, vol. 58, pp. 3247–61.
10. S. Fatemi-Varzaneh and A. Zarei-Hanzaki: *Mater. Sci. Eng. A*, 2009, vol. 504, pp. 104–06.
11. S. Fatemi-Varzaneh, A. Zarei-Hanzaki, J. Cabrera, and P. Calvillo: *Mater. Chem. Phys.*, 2015, vol. 149, pp. 339–43.
12. H. Wang, P. Wu, and J. Wang: *Comput. Mater. Sci.*, 2015, vol. 96, pp. 214–18.
13. J. Wang, D. Zhang, Y. Li, Z. Xiao, J. Fouse, and X. Yang: *Mater. Des.*, 2015, vol. 86, pp. 526–35.
14. H. Fan, S. Aubry, A. Arsenlis, and J.A. El-Awady: *Scripta Mater.*, 2015, vol. 97, pp. 25–28.
15. M. Quadir, M. Ferry, O. Al-Buhamad, and P. Munroe: *Acta Mater.*, 2009, vol. 57, pp. 29–40.
16. J. Del Valle, P. Rey, D. Gesto, D. Verdera, J.A. Jiménez, and O.A. Ruano: *Mater. Sci. Eng. A*, 2015, vol. 628, pp. 198–206.
17. M. Gzyl, A. Rosochowski, S. Boczkal, and L. Olejnik: *Mater. Sci. Eng. A*, 2015, vol. 638, pp. 20–29.
18. S. Biswas and S. Suwas: *Scr. Mater.*, 2012, vol. 66, pp. 89–92.
19. R.B. Figueiredo, S. Sabbaghianrad, A. Giwa, J.R. Greer, and T.G. Langdon: *Acta Mater.*, 2017, vol. 122, pp. 322–31.
20. W. Yuan, S. Panigrahi, J.Q. Su, R. Mishra: *Scr. Mater.*, 2011,.
21. J. Xing, X. Yang, H. Miura, and T. Sakai: *Mater. Trans.*, 2008, vol. 49, pp. 69–75.
22. Z. Zuberova, Y. Estrin, T. Lamark, M. Janecek, R. Hellmig, and M. Krieger: *J. Mater. Process. Technol.*, 2007, vol. 184, pp. 294–99.
23. W. Kim, C. An, Y. Kim, and S. Hong: *Scr. Mater.*, 2002, vol. 47, pp. 39–44.
24. H. Miura, G. Yu, and X. Yang: *Mater. Sci. Eng. A*, 2011, vol. 528, pp. 6981–92.

25. Y. Wang and E. Ma: *Acta Mater.*, 2004, vol. 52, pp. 1699–1709.
26. Q. Yang and A. Ghosh: *Acta Mater.*, 2006, vol. 54, pp. 5159–70.
27. N. Haghdadi, A. Zarei-Hanzaki, and D. Abou-Ras: *Mater. Sci. Eng. A*, 2013, vol. 584, pp. 73–81.
28. B. Bazaz, A. Zarei-Hanzaki, and S. Fatemi-Varzaneh: *Mater. Sci. Eng. A*, 2013, vol. 559, pp. 595–600.
29. S. Fatemi-Varzaneh and A. Zarei-Hanzaki: *Mater. Sci. Eng. A*, 2011, vol. 528, pp. 1334–39.
30. S. Fatemi-Varzaneh, A. Zarei-Hanzaki, M. Naderi, and A.A. Roostaei: *J. Alloys Compd.*, 2010, vol. 507, pp. 207–14.
31. S. Fatemi-Varzaneh, A. Zarei-Hanzaki, and J. Cabrera: *J. Allo. Comp.*, 2011, vol. 509, pp. 3806–10.
32. S. Fatemi-Varzaneh, A. Zarei-Hanzaki, and H. Paul: *Mater. Charac.*, 2014, vol. 87, pp. 27–35.
33. J.W. Cahn, Y. Mishin, and A. Suzuki: *Acta Mater.*, 2006, vol. 54, pp. 4953–75.
34. Y. Zhao, Y. Guo, Q. Wei, A. Dangelewicz, C. Xu, Y. Zhu, T. Langdon, Y. Zhou, and E. Lavernia: *Scripta Mater*, 2008, vol. 59, pp. 627–30.
35. W.F. Hosford and R.M. Caddell: *Metal Forming: Mechanics and Metallurgy*, Cambridge University Press, New York, 2011.
36. H. Somekawa and T. Mukai: *Philos. Mag. Lett.*, 2010, vol. 90, pp. 883–90.
37. C. Cepeda-Jiménez, J. Molina-Aldareguia, and M. Pérez-Prado: *Acta Mater.*, 2015, vol. 84, pp. 443–56.
38. M. Dahms and H.J. Bunge: *J. Appl. Crystallogr.*, 1989, vol. 22, pp. 439–47.
39. J. Koike: *Metall. Mater. Trans. A*, 2005, vol. 36, pp. 1689–96.
40. R. Lapovok, P. Thomson, R. Cottam, and Y. Estrin: *J. Mater. Sci.*, 2005, vol. 40, pp. 1699–1708.
41. S. Yin, C. Wang, Y. Diao, S. Wu, and S. Li: *J. Mater. Sci. Tech.*, 2011, vol. 27, pp. 29–34.
42. S. Agnew and Ö. Duygulu: *Int. J. Plast*, 2005, vol. 21, pp. 1161–93.
43. I. Saxl and I. Haslinggerová: *J. Phys. B*, 1974, vol. 24, pp. 1351–61.
44. S. Kleiner and P. Uggowitzer: *Mater. Sci. Eng. A*, 2004, vol. 379, pp. 258–63.
45. H. Somekawa and T. Mukai: *Metall. Mater. Trans. A*, 2015, vol. 46A, pp. 894–902.